



THE UNIVERSITY *of* EDINBURGH

## Edinburgh Research Explorer

### Pressure-induced amorphization and existence of molecular and polymeric amorphous forms in dense SO<sub>2</sub>

**Citation for published version:**

Zhang, H, Troth, O, Liu, X-D, Bini, R, Gregoryanz, E, Dalladay-Simpson, P, De Panfilis, S, Santoro, M, Gorelli, FA & Martonak, R 2020, 'Pressure-induced amorphization and existence of molecular and polymeric amorphous forms in dense SO<sub>2</sub>', *Proceedings of the National Academy of Sciences (PNAS)*.  
<https://doi.org/10.1073/pnas.1917749117>

**Digital Object Identifier (DOI):**

[10.1073/pnas.1917749117](https://doi.org/10.1073/pnas.1917749117)

**Link:**

[Link to publication record in Edinburgh Research Explorer](#)

**Document Version:**

Peer reviewed version

**Published In:**

Proceedings of the National Academy of Sciences (PNAS)

**General rights**

Copyright for the publications made accessible via the Edinburgh Research Explorer is retained by the author(s) and / or other copyright owners and it is a condition of accessing these publications that users recognise and abide by the legal requirements associated with these rights.

**Take down policy**

The University of Edinburgh has made every reasonable effort to ensure that Edinburgh Research Explorer content complies with UK legislation. If you believe that the public display of this file breaches copyright please contact [openaccess@ed.ac.uk](mailto:openaccess@ed.ac.uk) providing details, and we will remove access to the work immediately and investigate your claim.



# Pressure-induced amorphization and existence of molecular and polymeric amorphous forms in dense SO<sub>2</sub>

Huichao Zhang<sup>a,b</sup>, Ondrej Tóth<sup>c</sup>, Xiao-Di Liu<sup>a,2</sup>, Roberto Bini<sup>d</sup>, Eugene Gregoryanz<sup>a,e,f</sup>, Philip Dalladay-Simpson<sup>f</sup>, Simone De Panfilis<sup>g</sup>, Mario Santoro<sup>a,h,2</sup>, Federico Aiace Gorelli<sup>a,h,2</sup>, and Roman Martoňák<sup>c,2</sup>

<sup>a</sup>Key Laboratory of Materials Physics, Institute of Solid State Physics, Chinese Academy of Sciences, Hefei, 230031, China; <sup>b</sup>University of Science and Technology of China, Hefei 230026, China; <sup>c</sup>Department of Experimental Physics, Comenius University, Mlynská Dolina F1, 842 48 Bratislava, Slovakia; <sup>d</sup>Department of Chemistry Univ Florence and European Laboratory for non Linear Spectroscopy (LENS), via N. Carrara 1, 50019 Sesto Fiorentino, Italy; <sup>e</sup>School of Physics and Astronomy and Centre for Science at Extreme Conditions, University of Edinburgh, Edinburgh EH9 3JZ, UK; <sup>f</sup>Center for High Pressure Science Technology Advanced Research, 1690 Cailun Road, Shanghai, 201203, China; <sup>g</sup>Centre for Life Nano Science, Istituto Italiano di Tecnologia, viale Regina Elena 291, 00161 Rome, Italy; <sup>h</sup>Istituto Nazionale di Ottica (CNR-INO) and European Laboratory for non Linear Spectroscopy (LENS), via N. Carrara 1, 50019 Sesto Fiorentino, Italy

This manuscript was compiled on January 17, 2020

**We report here the pressure-induced amorphization and reversible structural transformation between two amorphous forms of SO<sub>2</sub>: molecular-amorphous and polymeric-amorphous, with the transition found at 26 GPa over a broad temperature regime, 77 - 300 K. The transformation was observed by both Raman spectroscopy and x-ray diffraction in a diamond anvil cell. The results were corroborated by *ab initio* molecular dynamics simulations, where both forward and reverse transitions were detected, opening a window to detailed analysis of the respective local structures. The high-pressure polymeric-amorphous form was found to consist mainly of disordered polymeric chains made of 3-coordinated sulfur atoms connected via oxygen atoms, with few residual intact molecules. This study provides an example of polyamorphism in a system consisting of simple molecules with multiple bonds.**

polyamorphism | sulfur dioxide | high pressure | polymeric form

Polyamorphism is the counterpart of polymorphism observed in crystalline solids. It is characterized by the existence of two or more disordered forms, either amorphous or liquid, differing in local structural order whilst preserving the stoichiometry. This phenomenon is often also accompanied by changes in coordination and density (1, 2) (for recent reviews see Refs. (3, 4)). Transformations between these different amorphous forms can be driven by pressure and temperature. While in the case of crystalline polymorphs the structural transitions are often (at least in principle) of first order and sharp, transitions in amorphous systems occur among isotropic forms and are more likely to be continuous. This is related to the absence of constraints prescribed by lattice periodicity, allowing for a gradual transformation between very different forms.

The first and perhaps most celebrated example of polyamorphic behavior was discovered in water ice by Mishima in 1984 (5, 6), observing that compression of ice I<sub>h</sub> at 77 K induced a transformation to an amorphous state. Through specific compression/decompression/heating protocols, at least two different forms of amorphous water ice were identified, known as low-density amorphous (LDA) and high-density amorphous (HDA) ices. The local structural order in the HDA and LDA ices differs by the presence of nonbonded water molecules in the first coordination shell of the former, resulting in the two forms having substantially different density. The existence of two amorphous forms of water ice was suggested to be related to existence of liquid-liquid transition and a second critical

point of water (7).

Since, similar phenomena have also been observed in other systems such as Si (8), SiO<sub>2</sub> (9–11), GeO<sub>2</sub> (12), where the polyamorphism is related to a change from tetrahedral to octahedral coordination at high pressure. Other examples where pressure induces changes in simple molecular systems include amorphous S (13) and liquid S (14) (for more examples and review see Refs. (3, 4)). Dramatic structural changes leading to amorphization have been observed upon compression of molecular crystals where multiple bonds are present. It is well known that pressure can destabilize multiple bonds in molecules in favour of extended polymeric networks with a higher coordination. Due to the associated strong kinetic effects, creation of amorphous phases are often observed, especially, when compression is performed at low temperatures. Amorphization of molecular crystals at high pressure have been observed in the famous examples of nitrogen (15, 16),

## Significance Statement

Some substances are known to exist in several different structurally disordered solid states and transform between them similarly to structural phase transitions between crystalline polymorphs. This interesting and yet not fully understood phenomenon is called polyamorphism and notable examples include water, SiO<sub>2</sub>, Si, etc. Here we present a new example of such behavior in a simple molecular substance, SO<sub>2</sub>. By using experimental high-pressure techniques we observe a reversible transition between different amorphous states around 26 GPa. Experimental results are well supported by *ab initio* simulations, which identify the high-pressure amorphous form as non-molecular, polymeric one consisting of intertwined chains. Our findings contribute to the fundamental understanding of structure of disordered matter as well as high-pressure behaviour of simple archetypal molecules.

H.C.Z. performed the experiments and contributed to the data analysis. O.T. performed simulations, analyzed the data and wrote the paper. X.D.L., R.B. and E.G. contributed to the discussion of results and wrote the paper. P.D.S. conducted the experiments and wrote the paper. X.D.L., P.D.S. and E.G. contributed materials/analysis tools. S.D.P. analyzed the data, contributed to the discussion of the results and wrote the paper. M.S. and F.A.G. designed the research, contributed to plan the experiments, to the data analysis and wrote the paper. R.M. designed the research, contributed to the analysis and discussion of results and wrote the paper.

The authors declare no conflict of interest.

<sup>2</sup>To whom correspondence may be addressed. Email: gorelli@lens.unifi.it, xiaodi@issp.ac.cn, santoro@lens.unifi.it or martonak@fmph.uniba.sk

carbon dioxide (17, 18) and benzene (19–21). In nitrogen, the strong triple bond of the molecule breaks under high pressures giving rise to a single-bonded network. Whilst in carbon dioxide, the double bond becomes unstable and carbon co-ordination increases to 3 and 4. In the case of benzene the aromatic ring opens and a network of hydrogenated carbons with single bonds is formed. The parent crystalline states of these amorphous materials have been discovered both in nitrogen (22, 23) and in carbon dioxide (24, 25) after high temperature annealing obtained by means of laser heating.

Sulphur dioxide is an important molecule in chemistry, serves a significant role in industrial applications, and has been attributed to atmospheric and geological processes. Unlike CO<sub>2</sub>, the SO<sub>2</sub> molecule is bent, described by two resonant structures with one single and one double bond(26, 27). The crystalline forms of SO<sub>2</sub> have been previously experimentally studied at pressures up to 32 GPa by Song et al.(28). Here, we present a combined experimental and computational study of SO<sub>2</sub> up to pressures of 60 GPa and over a broad temperature regime. Observations via Raman spectroscopy and X-ray diffraction, well supported by *ab initio* simulations, provide a detailed description on the atomistic level of the transformations under compression/decompression cycles. These findings give evidence of a hitherto unobserved example of polyamorphism related to a reversible transformation between molecular and polymeric amorphous forms of SO<sub>2</sub>.

In Fig. 1, we present a selection of Raman spectra measured upon increasing pressure up to 60 GPa, at 77 K (panel A), as well as subsequent decompression back to ambient pressure at room temperature (panel B). Similar experiments for compressions at 210 K were also conducted and reported in Fig. S1 Supp. Mat. We find in general, an agreement between our Raman measurements of solid molecular SO<sub>2</sub> under pressure and those reported previously (28). However, the dramatic spectral changes at low temperatures were not observed previously as pressures were limited to only 22 GPa (28). From these datasets, what is readily evident is the progression from sharp molecular peaks of SO<sub>2</sub>, i. e.  $\nu_1$  1050-1220 cm<sup>-1</sup>,  $\nu_3$  1240-1320 cm<sup>-1</sup> and  $\nu_2$  520-600 cm<sup>-1</sup>, to much broader, weaker peaks upon compression. In addition, new broad and weak bands appear at different frequencies, characteristics which are compatible with pressure-induced amorphization together with major changes in the local structure. Further, the well-defined molecular peaks of SO<sub>2</sub> are recovered upon decreasing pressure, while the new broad bands disappear, demonstrating that these changes are indeed reversible and are therefore incompatible with any irreversible processes, such as chemical decomposition (SO<sub>2</sub> → S + O<sub>2</sub>).

Taking a detailed analysis of the spectra, we can shed light on a number of remarkable features. We find that the numerous sharp lattice peaks, observed below 300-400 cm<sup>-1</sup>, weaken above 16 GPa until they become undetectable above 21 GPa at 77 K (Fig. 1 A) or above 10 GPa at 210 K (Fig. S1 Supp. Mat.), and instead are replaced by a new broad band in the same spectral region. However, at higher frequencies, under the same conditions, we do not observe any additional peaks other than the molecular peaks,  $\nu_1$ ,  $\nu_2$ , and  $\nu_3$ , of SO<sub>2</sub> up to 25 GPa. The linewidth of the crystal peaks severely increases upon growing pressure while the intensity decreases substantially. These spectral changes are highly indicative that upon cold compression above 10-15 GPa, crystalline molecular

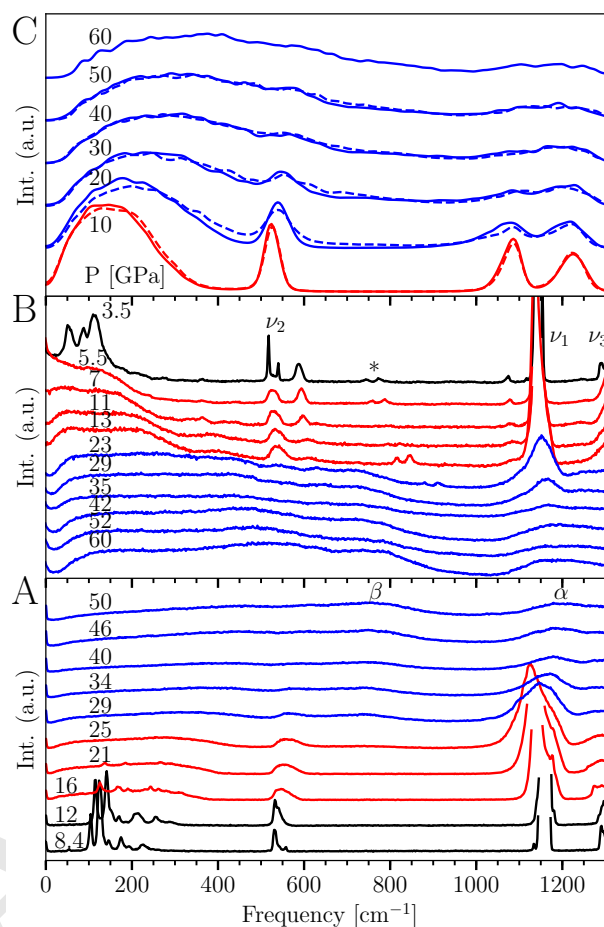


**Fig. 1.** Vibrational spectra of solid SO<sub>2</sub>. Panels A and B: selected Raman spectra of an SO<sub>2</sub> sample measured upon increasing pressure at 77 K (A) and decreasing pressure at room temperature (B). During compression, the initially sharp molecular peaks of SO<sub>2</sub>,  $\nu_1$ ,  $\nu_2$ , and  $\nu_3$ , broaden and become very weak while new broad and weak bands appear at different frequencies, indicating pressure-induced amorphization together with changes in the local structure. Upon decompression, the sharp molecular peaks of SO<sub>2</sub>,  $\nu_1$ ,  $\nu_2$ , and  $\nu_3$ , are recovered while the new broad bands disappear at the same time, showing that amorphization and overall changes in the local structure are reversible. Panel C: evolution of vibrational density of states (VDOS) from *ab initio* MD simulations along compression (solid lines) and decompression (dashed lines). Color represents structural state of the system: black - molecular crystal, red - molecular amorphous and blue - polymeric amorphous. Star in panel B marks ruby peaks.

SO<sub>2</sub> undergoes a structural transformation into an amorphous form whilst preserving its molecularity, i. e. consisting of SO<sub>2</sub> molecular units. Amorphization could have been enhanced by the shear stress, which is in turn related to the deformation of the gasket hole. This is supported also by our DFT calculations (see section on simulation results). Upon further compression, above 22-25 GPa, additional and significant modifications to the Raman signature are observed, the  $\nu_2$  and  $\nu_3$  peaks progressively diminish and are barely observable above 30-34 GPa. Conversely, the strongest Raman excitation of SO<sub>2</sub>,  $\nu_1$  (1170-1200 cm<sup>-1</sup> (Fig. 1 A)), is visible to the maximum pressures of 50-60 GPa (see also Fig. 1 B), albeit comparatively weaker. The  $\nu_1$  band peak is found to merge with an altogether new weak and broad peak centred at 1220-1230 cm<sup>-1</sup>, denoted as  $\alpha$  in Fig. 1 A. In addition to emergence of the  $\alpha$ -peak, another new and broad band appears, at 600-1000 cm<sup>-1</sup> with

a high frequency edge at around 900  $\text{cm}^{-1}$ , which we call  $\beta$ . Both bands  $\alpha$  and  $\beta$  appear to be of non-molecular origin, which suggests that the emergence of these excitations signals that amorphous-molecular  $\text{SO}_2$  undergoes a transformation into a non-molecular/extended amorphous form.

Comparison with the pressure-induced molecular to amorphous-non-molecular transformation in  $\text{CO}_2$  (17, 18, 25) can help to interpret the transformation observed here in  $\text{SO}_2$ , as it bears similarities. Carbonia, the non-molecular amorphous  $\text{CO}_2$ , has been shown to be made of a mixture of C in a 3-fold and 4-fold oxygen coordination in similar proportions. The 3-fold coordinated C sites are uniquely identified by C=O stretching peaks in the Raman and the IR spectrum, 1900-2000  $\text{cm}^{-1}$  at 50-60 GPa, which roughly corresponds to the average value,  $\nu(\text{stretch CO}_2)$ , between the symmetric and the antisymmetric stretching modes of molecular  $\text{CO}_2$ . However, when considering the full Raman and IR spectra, the single C-O bond stretching and deformation modes ascribed to both 3-fold and 4-fold coordinated C sites, form a broad spectral distribution extending over 500-1500  $\text{cm}^{-1}$ , approximately 0.26-0.77 of the average  $\nu(\text{stretch CO}_2)$ . Consequently, in the case of  $\text{SO}_2$ , the aforementioned peak,  $\alpha$ , is roughly the average frequency of the two molecular stretching modes, and can therefore be attributed to the S=O stretching modes for non-molecular/extended  $\text{SO}_2$  with S in 3-fold coordination by O. In addition, in the frequency range given by 0.26-0.77 of  $\alpha$ , 320-940  $\text{cm}^{-1}$ , we observe the previously described band  $\beta$ . Therefore, again in accordance with the  $\text{CO}_2$  analogue, the  $\beta$  band can be attributed to single S-O bond stretching and deformation modes in the non-molecular/extended  $\text{SO}_2$ . A discrepancy of using carbonia as an analogue however is that the 4-fold oxygen coordination is absent in  $\text{SO}_2$ , in accordance with our DFT simulations (discussed later). We do however also have a two component system, considering that the  $\nu_1$  peak for molecular  $\text{SO}_2$  is still present at the highest pressures, although weak. Therefore, inferring that the overall non-molecular/extended  $\text{SO}_2$  consists of a mixture of trace 2-fold S sites, still molecular in nature, in a bulk of non-molecular 3-fold coordinated S sites. An alternative possibility compatible with experimental data would be that molecular parts of the sample with 2-fold coordinated S and non-molecular parts with S in higher coordination are phase separated on a macroscopic/mesoscopic scale.

On decompression, the spectral changes and transformations identified previously on compression are reverted, demonstrated in Fig. 1 B. However, a minor hysteresis is observed, attributed to the kinetically limited structural changes. We observe that when the sample is decompressed below 30-25 GPa, both the  $\alpha$  peak and  $\beta$  band disappear, whilst the well-defined molecular peaks  $\nu_1$ ,  $\nu_2$ , and  $\nu_3$  emerge suddenly. Further, in the low frequency/lattice region below 350  $\text{cm}^{-1}$  a diffuse, liquid-like band clearly develops, with no additional substantial changes down to about 5 GPa. These changes demonstrate again a change in the amorphous structure, recovering molecular  $\text{SO}_2$  units at 25-5 GPa on decompression. This molecular-amorphous phase is then found to further transform into a crystalline molecular  $\text{SO}_2$  structure below 5 GPa, indicated by the sharp lattice mode peaks observed below this pressure and crystalline x-ray diffraction (discussed later). Interestingly, an additional peak is found below 20 GPa at around 600  $\text{cm}^{-1}$  which was also observed in a previous study,

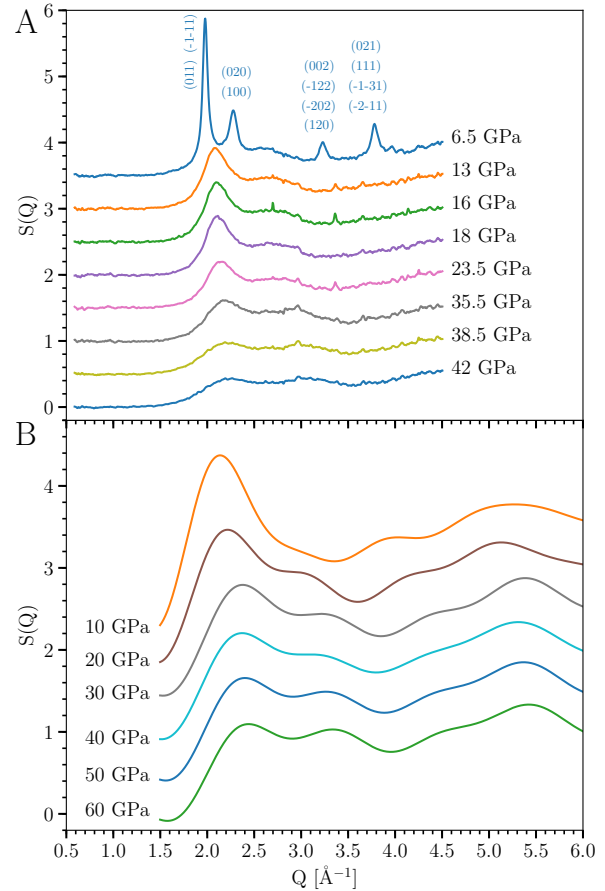


**Fig. 2.** Static structure factor of solid  $\text{SO}_2$  under pressure. Panel A: experimental  $S(Q)$  measured along a room temperature decompression run, panel B:  $S(Q)$  computed from simulations at 300 K during decompression (the graph computed from simulation of compression is in Supp. Mat. Fig. S2. Region of  $S(Q)$  beyond  $4.5 \text{ \AA}^{-1}$  in A is inaccessible because of limited angle in experiment, while the region below  $1.5 \text{ \AA}^{-1}$  in B is not reliable because of limited RDF range, resulting from the simulation supercell size of  $14 \text{ \AA}$ . The Bragg peaks have been indexed on the basis of a  $Aea2$  space group with  $a=5.5430 \text{ \AA}$ ,  $b=5.4011 \text{ \AA}$ ,  $c=5.5356 \text{ \AA}$  as obtained from simulations (see also Fig. S11 in Supp. Mat.).

where it was attributed to the formation of molecular clusters (28). The reversible transformations of  $\text{SO}_2$  to molecular and non-molecular amorphous forms again parallel the similar case of  $\text{CO}_2$  (17, 18, 25), and at odds with the cases of aromatic molecules, where instead amorphous non-molecular forms obtained at high pressures are recoverable to ambient conditions (19-21, 29, 30).

The non-crystalline nature of  $\text{SO}_2$  at high pressure has also been assessed by x-ray diffraction, and the evolution of the static structure factor upon room temperature decompression of sample compressed at low temperature is shown in Fig. 2 A. The static structure factor has been obtained by the empty cell subtraction, taking into account the form factors of oxygen and sulfur as well as the Compton contribution from the sample, following a procedure described elsewhere (31). In general, it is found that at the highest pressures the two peaks at about  $2.2$  and  $3 \text{ \AA}^{-1}$  are of similar intensity, while on decompression the first peak significantly increases with respect to the second one which at the same time moves to lower  $Q$ . Critically, in



comparison between patterns measured at 35.5 and 23.5 GPa, there is a clear change of the static structure factor. The first contribution, centred at  $2.2 \text{ \AA}^{-1}$ , becomes more prominent and sharpens markedly, whilst the second has a more subtle loss of intensity. These changes, corresponding to the transformation from an extended amorphous to a molecular amorphous form, are in strong agreement with the Raman results outlined previously.

In summary, we have observed two distinct structural transformations. At lower pressures, the transformation from a molecular crystal to a molecular, van der Waals type, amorphous solid, with no changes in the molecular unit and to a non-molecular/extended state on further compression. Interestingly, a substantial effect of temperature is observed for the former transformation, despite the expected energy barrier to be comparatively small. For example, instead of an expected isobaric phase line, the transformation occurs at 5 GPa lower pressures at 210 K compared with 77 K isotherm. Conversely, the second transformation, to a non-molecular/extended amorphous state, is a chemically reconstructive one, and therefore would logically have a higher associated energy barrier and consequently a stronger temperature dependence. Instead, this transformation is observed at roughly the same pressures for both isotherms studied, 77 K and 210 K, at around 25-30 GPa, counterintuitively suggesting that the barrier for polymerization is small in relation to the initial molecular amorphisation. We note that this is quite different from the case of  $\text{CO}_2$  and  $\text{N}_2$ , where a much stronger hysteresis is reported (23–25).

In order to obtain a better understanding of the processes on the atomistic level, we performed *ab initio* MD simulations following a pressure path akin to the experiment. We first performed a test in order to check whether applying shear stress to a perfect *Aea2* molecular crystal at low pressure might result in amorphous molecular structure as observed in experiments. We gradually induced shear strain by deforming the  $\gamma$  angle of the supercell by up to  $30^\circ$  and observed transformation into a disordered molecular form, confirming the experimentally observed amorphization.

The full simulation protocol is shown in Fig. S3 in Supp. Mat. In order to start the compression from a well-defined amorphous molecular structure, we melted a perfect *Aea2* molecular crystal (32) in a  $3 \times 3 \times 3$  supercell (108  $\text{SO}_2$  molecules, equivalent to a 324 atom unit cell) by heating at  $P = 0$  GPa to 600 K. Through subsequent cooling to 0 K, we prepared the amorphous structure, which served as an initial configuration for further simulations. Following the experimental pathway, we performed a gradual compression to 60 GPa and subsequent decompression to 10 GPa (in 10 GPa steps) at 300 K in order to accelerate the structural transformations (both on compression and decompression). Interestingly, at this temperature we observed some diffusion of molecules in the molecular phase, suggesting that the sample might possibly be in metastable liquid regime.

Analysis of the partial radial distribution functions (RDFs) (Fig. 3), obtained from simulations, can provide a more detailed description of the observed transformations on an atomistic level. The RDFs clearly indicate the reversible amorphous to amorphous transformation, corresponding to the S in 2- to 3-fold O coordination change, providing further evidence for the experimentally observed phases and their associated reversibility. Upon compression of the initial molecular amor-

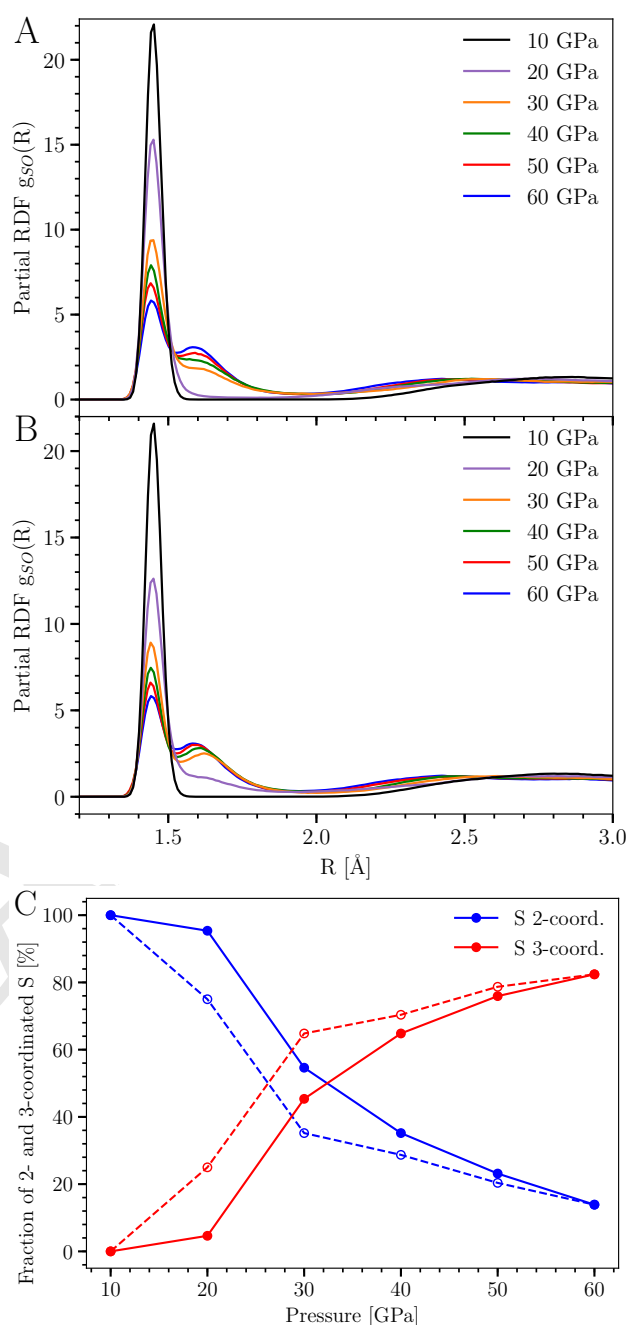


**Fig. 3.** Partial S-O radial distribution function (RDF) and concentration of sulfur coordination states. Panel A: RDF during compression, panel B: RDF during decompression and panel C: fraction of 2- and 3-coordinated S atoms during compression (solid line) and decompression (dashed line). Coordination number was determined within the cutoff of 1.92 Å.

phous sample to 10 GPa at 300 K,  $\text{SO}_2$  retains its molecular units. Evidenced in Fig. 3 A, the peak at 1.44 Å, corresponding to the double bond, is sharp and well separated from the next neighbor at 2.5-3.0 Å and the coordination number of S atoms with respect to O atoms is 2. Upon compression to 20 GPa modifications in the RDF are observed, and at 30 GPa there is a substantial change, the first peak becomes weaker whilst a new peak at slightly longer distance, 1.6 Å, appears. These changes indicate that some of S=O double bonds are

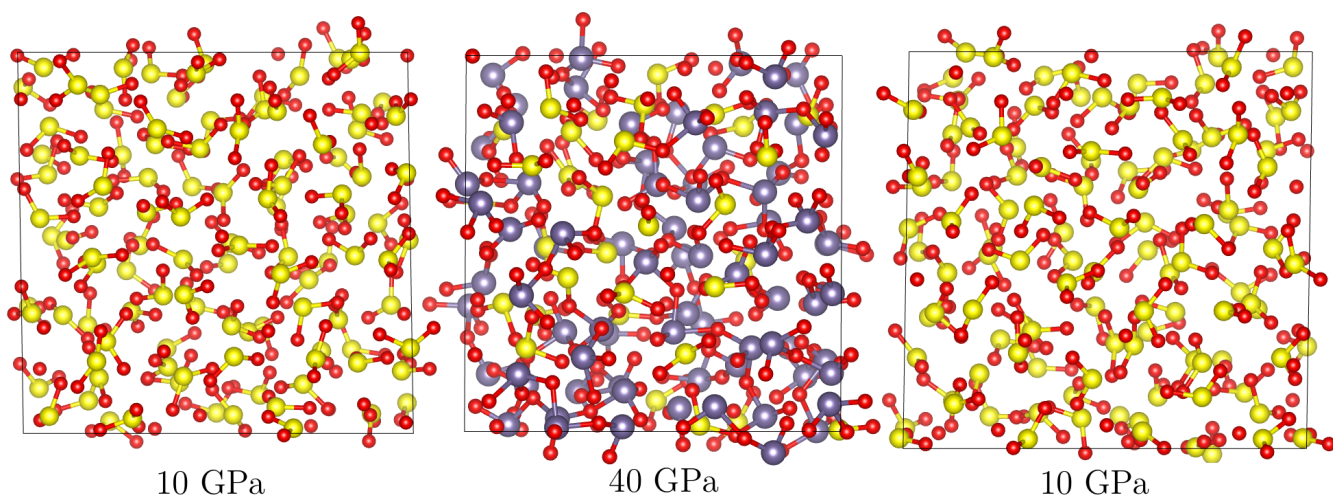


**Fig. 4.** Snapshots of the simulated sample at different pressures. Left panel: the beginning of compression at 10 GPa where sample consists only of  $\text{SO}_2$  molecules. Middle panel: structure during compression at 40 GPa with S atoms colored by coordination: 2-yellow (molecule) and 3-gray (polymeric chains). Right panel: structure after decompression to 10 GPa reverted from polymeric back to molecular. Simulation supercells are not to scale.

broken and replaced by single ones. In the same pressure regime, 3-coordinated S-atoms appear with 2 single S-O bonds and one S=O double bond, forming polymeric chains (see snapshots shown in Fig. 4). On further compression, the first peak is found to progressively diminish in intensity whilst the second is enhanced, resulting in 82 % of S atoms to be in a 3-fold oxygen coordination at 60 GPa. On decompression (see Fig. 3 B), akin to experimental observations, we observed the reverse evolution, further demonstrated by the pressure dependence of the number of 2- and 3-coordinated S atoms in Fig. 3 C. Additionally, at 10 GPa the previously identified polymeric chains observed on compression disappear entirely (see Fig. 4), and the system reverts back to its initial molecular amorphous state. The strong agreement between experiment and simulations, means that insights from the MD-calculations can identify the experimental observations as forward and backward transitions between molecular and polymeric amorphous forms of  $\text{SO}_2$ . The dependence of the coordination number of S atoms on pressure (Fig. 3 C) exhibits some hysteresis, which suggests that the transition might have a weakly first-order character. The pressure dependence of density upon compression and decompression, shown in Fig. S4 (Supp. Mat.) shows a very small hysteresis and does not exhibit any particular features across the structural transformation. We performed a similar compression simulation also at 500 K and found the polymerization to start at 30 GPa, suggesting that the transition is shifted to higher pressure upon increasing temperature.

Above 20 GPa, the calculated static structure factor,  $S(Q)$ , shows important changes upon compression (Fig. S2 Supp. Mat.). The intensity of the first diffraction peak at about  $2.2 \text{ \AA}^{-1}$  drops, while a new peak appears, around  $3 \text{ \AA}^{-1}$ , which grows with increasing pressure. At 60 GPa, the height of both peaks becomes similar, reflecting XRD patterns above 35.5 GPa in Fig. 2 A. All changes are found to be reversible upon decompression, albeit with a small hysteresis, and the calculated structure factor agrees very well with the experimental one (Fig. 2). Simulations allow us to decompose the total  $S(Q)$  into contributions from atomic pairs (Figs. S5 Supp. Mat.) The first peak, around  $2.2 \text{ \AA}^{-1}$ , originates mainly from

non-bonded S...S pairs, while the weaker second peak, at  $3 \text{ \AA}^{-1}$ , comes from O...O and finally the broad peak, around  $5 \text{ \AA}^{-1}$ , is mainly due to the S-O pairs. It is clear that the loss of the first peak of total  $S(Q)$  is a consequence of changes in the S-O contribution, which exhibits a pronounced drop above 20 GPa (Fig. S5 Supp. Mat.). Therefore, the observed evolution of  $S(Q)$  can directly reflect changes of the distance of S-O neighbors upon polymerization.

On compression, comparing the vibrational spectra from simulations (Fig. 1 C) with experimental Raman spectra (Fig. 1 A), we observe qualitatively similar evolution. Above 20 GPa the distinct  $\nu_2$  peak at  $550 \text{ cm}^{-1}$  progressively disappears whilst the  $400 - 500$  and  $600 - 900 \text{ cm}^{-1}$  regions become enhanced. Meanwhile, the two molecular peaks,  $\nu_1$  around  $1100 \text{ cm}^{-1}$  and  $\nu_3$  above  $1200 \text{ cm}^{-1}$  gradually merge into a single broad peak around  $1200 \text{ cm}^{-1}$ , again in agreement with experiments (Fig. 1 A). The evolution of the peaks can be understood from the projected VDOS, allowing decomposition of the total VDOS into contributions from structurally distinct S and O atoms (Fig. S6 Supp. Mat.). Both S and O atoms can be either in molecules or in polymeric chains. Moreover, O atoms in polymeric chains are either at a bridging position between two S atoms (S-O-S) or at terminal position, doubly bonded to S atoms (S=O). The evolution of the total VDOS clearly reflects the gradual conversion of molecules into polymeric chains. Again, upon decompression the reverse evolution is observed, in agreement with experiment (Fig. 1 B).

In order to understand the origin of the two amorphous phases it is useful to discuss their underlying crystalline counterparts.  $\text{SO}_2$  forms at ambient pressure and low temperature below 201 K, an *Aea2* molecular crystal (32). Instead, its analogue  $\text{SeO}_2$  forms at ambient pressure a *P42/mbc* polymeric crystal consisting of chains (mineral Downeyite (33)). The possible existence of polymeric  $\text{SO}_2$  (polysulfite) was studied in Refs. (34, 35) where energies of various oligomers were calculated. Additionally, in Ref. (35) a crystal structure with infinite polymeric chains was studied obtained by substituting Se atoms in Downeyite by S atoms. It was concluded that polymeric  $\text{SO}_2$  is energetically higher than its molecular form and it was proposed that the polymer could be stabilized at

high pressure. This can be understood by applying the well-known pressure-homology rule(36), (37), (38) stating that light elements behave at high pressure like more heavy elements from the same group at lower pressures.

The structure of polymeric phases of SO<sub>2</sub> has not been, to our knowledge, determined experimentally. In order to check its possible existence at high pressure we performed a structural search of crystalline phases of SO<sub>2</sub> employing evolutionary approach (details are described in Methods). We show here the main results of our search. The enthalpy vs. pressure graph for low-enthalpy phases is shown in Supp. Mat. Fig. S7. At zero pressure we found the molecular crystal structure with space group *Aea2*, in agreement with experiment(32). Upon increasing pressure we found another molecular crystal structure *P2<sub>1</sub>/c* which becomes stable above 1 GPa. Besides this structure there are two low-lying metastable molecular structures *Pc*, and *Cc*, which around 11 GPa transform into different molecular forms with space groups *Pmc2<sub>1</sub>* and *Ama2*, respectively and become stable (both have very similar enthalpies) with respect to the *P2<sub>1</sub>/c* one. Upon further compression they transform into polymeric structures (all structures are shown in Supp. Mat. Fig. S8 and cif files of the *Pmc2<sub>1</sub>* and *Ama2* structures are included in Supp. Mat.). Both polymeric structures still have very similar enthalpy and conformation of chains and differ only in chain stacking. The mechanism of polymerization is illustrated in Fig. S9 Supp. Mat. showing the pressure evolution of bond-lengths upon compression. A similar polymerization mechanism is likely to apply also in the amorphous phase when molecules of suitable orientation approach each other. Both polymeric structures have the same conformation of chains as SeO<sub>2</sub> downeyite but the stacking of chains is different. The stable polymeric structure has at 20 GPa bond length of 1.46 Å between S atom and terminal oxygen (S=O) and 1.65 Å between S atom and bridging oxygen (S-O), similar to the peak positions of S-O RDF (Fig. 3). The sulphur atom in the chain is surrounded by three oxygen atoms in roughly trigonal pyramid coordination (at 20 GPa bond angle O-S-O is 90° and O=S-O is 100°) suggesting presence of sp<sup>3</sup> hybridization (see also Ref.(35) where it was suggested that the dimerization of SO<sub>2</sub> is related to sp<sup>2</sup> → sp<sup>3</sup> rehybridization). In order to quantitatively assess the bond order of S O bonds in molecular and polymeric SO<sub>2</sub> we employed the DDEC6 atomic population analysis method(39). We found a bond order of 2.12 in molecule and 2.14 and 1.15 for S=O and S-O bonds in the polymeric phase. In Fig. S10 Supp. Mat. we show the e-DOS including projections on *s* and *p* orbitals for the crystalline molecular and polymeric phase (no *d*-orbital participation was found). We also note that the diffraction pattern of the recrystallized phase upon decompression to 6.5 GPa (Fig.2 A) shows a strong similarity with the diffraction pattern of the molecular phase *Aea2* at the same pressure (for comparison see Fig. S11 Supp. Mat.). This provides an additional evidence that the system after the compression/decompression cycle returns to its parent state.

To assess quantitatively the effects of structural disorder, we calculated the enthalpy of the amorphous phase (relaxed to *T* = 0) and found it at 10 GPa to be about 0.26 eV/formula unit above the crystalline phases (it is shown in Fig. S7 in Supp. Mat.). We note that because of the short time scale available in the ab initio MD simulations (of the order of 10 ps) the amorphous structure might not be fully relaxed

structurally. We also determined with our DFT simulations the electronic properties of the a-SO<sub>2</sub> phase. The system does not metalize up to 60 GPa, with band gap of at least 0.6 eV in PBE approximation.

**Conclusions and outlook.** We observed a pressure-induced amorphization and a reversible structural transition between molecular and polymeric amorphous forms of SO<sub>2</sub> at pressures around 26 GPa. The transition has small hysteresis pointing to the fact that the associated kinetic barriers are low. The lower pressure of the transition between molecular and polymeric amorphous forms, as well as the back transformation, is qualitatively facilitated by the molecular polarity. This, supported by the high density attainable under pressure, drives the intermolecular interaction and lowers the activation energy of the transformation. To our knowledge this kind of transition was not yet observed and provides a new example of structural transition between disordered non-equilibrium states of solid matter. Unlike in a-CO<sub>2</sub>, where polymeric a-carbonia contains 3- as well as 4-coordinated C atoms, here the molecular form converts into polymeric form with only 3-coordinated S atoms. It will be of interest to study whether the two amorphous states continue to exist also in liquid state, either in stable or metastable (undercooled) region. Further experimental and theoretical work is necessary to accurately map the solid and liquid regions and uncover further details of the phase diagram of SO<sub>2</sub>.

## Materials and Methods

**Experimental methodology.** The SO<sub>2</sub> gas was loaded into the DAC by means of cryogenic loading; the gas was condensed between one diamond anvil and the gasket placed on the other diamond of a DAC which was opened by few mm and cooled to liquid nitrogen temperature inside a sealed glove box purged with nitrogen to avoid moisture condensation. We performed Raman spectroscopy using a state of the art confocal Raman microscope with 15 and 2 micron of axial and transverse resolution respectively. The spectrometer consisted of a Spectra Pro 750 mm monochromator, equipped with Pixis Princeton Instrument CCD detector. Bragg grating filters were used to attenuate the laser light and spatial filtering of the collected light to obtain high quality spectra down to 7 cm<sup>-1</sup> with minimal background from the diamond anvils and strong signal from the sample. The laser beam was expanded and cleaned by a Band Pass Filter. We used a Laser Torus at 660 nm with 10 mW of power and Laser Ventus at 532 nm with 0.5 mW of power to check for the presence of eventual fluorescence bands in the spectrum. We generally used a 300 gr/mm grating as the spectral features were getting very broad and weak with pressure. The pressure was determined by the fluorescence of a small ruby placed in the sample or from the diamond stressed edge which we detect with high accuracy thanks to the excellent spatial resolution of the setup. The XRD measurements were made at Petra (proposal ID: I-20181128) using monochromatic X-ray beam with 42.7 keV energy ( $\lambda = 0.2922$  Å) and the scattered X-rays were detected by a Perkin Elmer XRD1621 (2048x2048 pixels, 200x200um) detector. The diffraction patterns have been measured only along decompression of an amorphous sample obtained from a compression at low temperature while monitoring the changes with Raman spectroscopy. The excellent transverse spatial resolution allows to obtain clean diffraction patterns of the sample without the presence of spurious diffraction lines from the metallic gasket. The empty cell subtraction, which is of fundamental importance to obtain reliable measurements of the diffuse scattering from an amorphous or liquid sample in the DAC, has been in this case easily obtained by measuring the empty cell at the end of the decompression run when the SO<sub>2</sub> has completely back transformed to the gas state and escaped from the sample chamber.



**Simulations methodology.** We performed a structural search for crystalline phases of  $\text{SO}_2$  employing the USPEX (40) package at pressures 10, 20 and 50 GPa with 4 formula units (12 atoms) within unit cell. *Ab initio* simulations were performed by density functional theory (DFT) as implemented in VASP 5.3 and 5.4 codes (41–43), employing projector augmented-wave pseudopotentials (with 6 valence electrons for both S and O atoms) and Perdew-Burke-Ernzerhof (PBE) (44) parametrization of the GGA exchange-correlation functional. In evolutionary search, structural relaxations and enthalpy calculations we employed the harder  $\text{S}_\text{h}$  and  $\text{O}_\text{h}$  pseudopotentials with cutoff of 910 eV while in MD calculations we used the regular ones S and O with cutoff of 520 eV. Compression, decompression and heating were performed by 6 ps variable cell NpT simulations with Langevin thermostat and  $\Gamma$ -point Brillouin zone sampling. We used 10.0 and 2.0  $\text{ps}^{-1}$  friction coefficients for atomic and lattice degrees of freedom respectively, and 10000  $m_u$  as barostat fictitious mass. Data for velocity autocorrelation function were generated by equilibrating sample for 6 ps in NpT and then running 20 ps NVE simulation. Total and projected vibrational density of states (VDOS) were computed in standard way as Fourier transform of mass-weighted velocity autocorrelation function from MD trajectories at pressures from 10 to 60 GPa. Static structure factors  $S(Q)$  were calculated by performing Fourier transform of the RDFs from MD trajectories at several pressures along compression and decompression runs.

**ACKNOWLEDGMENTS.** RM acknowledges stimulating discussions with P. Mach. RM and OT were supported by the Slovak Research and Development Agency under Contract No. APVV-15-0496. Calculations were performed at the Computing Centre of the Slovak Academy of Sciences using the supercomputing infrastructure acquired in ITMS Projects No. 26230120002 and No. 26210120002 (Slovak Infrastructure for High-Performance Computing) supported by the Research and Development Operational Programme funded by the ERDF. Experimental part was supported by the CAS President's International Fellowship Initiative (PIFI), No. 2018VMA0053, and No. 2019VMA0027, National Natural Science Foundation of China (Grant Nos. 11874361, 51672279, 11774354 and 51727806), Science Challenge Project (No. TZ2016001), and the CASHIPS Director's Fund (Grant No. YZJJ2017705).

1. PH Poole, TT Grande, CA Angell, PF McMillan, Polymorphic phase transitions in liquids and glasses. *Science* **275**, 322–323 (1997).
2. PF McMillan, Polyamorphic transformations in liquids and glasses. *J. Mater. Chem.* **14**, 1506–1512 (2004).
3. D Machon, F Meersman, M Wilding, M Wilson, P McMillan, Pressure-induced amorphization and polyamorphism: Inorganic and biochemical systems. *Prog. Mater. Sci.* **61**, 216 – 282 (2014).
4. MA Anisimov, et al., Thermodynamics of fluid polyamorphism. *Phys. Rev. X* **8**, 011004 (2018).
5. O Mishima, LD Calvert, E Whalley, 'melting ice' i at 77 k and 10 kbar: a new method of making amorphous solids. *Nature* **310**, 393–395 (1984).
6. O Mishima, LD Calvert, E Whalley, An apparently first-order transition between two amorphous phases of ice induced by pressure. *Nature* **314**, 76–78 (1985).
7. PH Poole, F Sciortino, U Essmann, HE Stanley, Phase behaviour of metastable water. *Nature* **360**, 324–328 (1992).
8. PF McMillan, M Wilson, D Daisenberger, D Machon, A density-driven phase transition between semiconducting and metallic polyamorphs of silicon. *Nature* **4**, 680–684 (2005).
9. M Grimsditch, Polymorphism in Amorphous  $\text{SiO}_2$ . *Phys. Rev. Lett.* **52**, 2379–2381 (1984).
10. RJ Hemley, AP Jephcoat, HK Mao, LC Ming, MH Manghnani, Pressure-induced amorphization of crystalline silica. *Nature* **334**, 52–54 (1988).
11. Q Williams, R Jeanloz, Spectroscopic evidence for pressure-induced coordination changes in silicate glasses and melts. *Science* **239**, 902–905 (1988).
12. DJ Durben, GH Wolf, Raman spectroscopic study of the pressure-induced coordination change in  $\text{geO}_2$  glass. *Phys. Rev. B* **43**, 2355–2363 (1991).
13. C Sanloup, E Gregoryanz, O Degtyareva, M Hanfland, Structural transition in compressed amorphous sulfur. *Phys. Rev. Lett.* **100**, 075701 (2008).
14. L Henry, et al., A density-driven first-order phase transition in liquid sulfur. *arXiv e-prints*, arXiv:1709.09996 (2017).
15. AF Goncharov, E Gregoryanz, H Mao, Z Liu, R Hemley, Optical evidence for a nonmolecular phase of nitrogen above 150 gpa. *Phys. review letters* **85**, 1262–5 (2000).
16. E Gregoryanz, AF Goncharov, R Hemley, H Mao, High-pressure amorphous nitrogen. *Phys. Rev. B* **64** (2001).

17. M Santoro, et al., Amorphous silica-like carbon dioxide. *Nature* **441**, 857–860 (2006).
18. JA Montoya, R Rousseau, M Santoro, F Gorelli, S Scandolo, Mixed threefold and fourfold carbon coordination in compressed  $\text{CO}_2$ . *Phys. Rev. Lett.* **100**, 163002 (2008).
19. L Ciabini, M Santoro, R Bini, V Schettino, High pressure reactivity of solid benzene probed by infrared spectroscopy. *The J. Chem. Phys.* **116**, 2928–2935 (2002).
20. L Ciabini, M Santoro, R Bini, V Schettino, High pressure photoinduced ring opening of benzene. *Phys. review letters* **88**, 085505 (2002).
21. L Ciabini, et al., Triggering dynamics of the high-pressure benzene amorphization. *Nature* **6**, 39 (2007).
22. C Mailhot, LH Yang, AK McMahan, Polymeric nitrogen. *Phys. Rev. B* **46**, 14419–14435 (1992).
23. MI Eremets, AG Gavriliuk, IA Trojan, DA Dzivenko, R Boehler, Single-bonded cubic form of nitrogen. *Nature* **3**, 558–563 (2004).
24. F Datchi, B Mallick, A Salamat, S Ninet, Structure of polymeric carbon dioxide  $\text{CO}_2$  – V. *Phys. Rev. Lett.* **108**, 125701 (2012).
25. M Santoro, et al., Partially collapsed cristobalite structure in the non molecular phase v in  $\text{CO}_2$ . *Proc. Natl. Acad. Sci.* **109**, 5176–5179 (2012).
26. JE House, *Inorganic Chemistry*. (Academic Press), (2008).
27. TY Takeshita, BA Lindquist, TH Dunning, Insights into the electronic structure of ozone and sulfur dioxide from generalized valence bond theory: Bonding in  $\text{O}_3$  and  $\text{SO}_2$ . *The J. Phys. Chem. A* **119**, 7683–7694 (2015) PMID: 26068052.
28. Y Song, Z Liu, H Mao, RJ Hemley, DR Herschbach, High-pressure vibrational spectroscopy of sulfur dioxide. *The J. Chem. Phys.* **122**, 174511 (2005).
29. M Ceppatelli, M Santoro, R Bini, V Schettino, High pressure reactivity of solid furan probed by infrared and raman spectroscopy. *The J. Chem. Phys.* **118**, 1499–1506 (2003).
30. M Santoro, M Ceppatelli, R Bini, V Schettino, High-pressure photochemistry of furane crystal. *The J. Chem. Phys.* **118**, 8321–8325 (2003).
31. JH Eggert, G Weck, P Loubeyre, M Mezouar, Quantitative structure factor and density measurements of high-pressure fluids in diamond anvil cells by x-ray diffraction: Argon and water. *Phys. Rev. B* **65**, 174105 (2002).
32. B Post, RS Schwartz, I Fankuchen, The crystal structure of sulfur dioxide. *Acta Crystallogr.* **5**, 372–374 (1952).
33. Kenny, Stähli, The crystal structure of  $\text{SeO}_2$  at 139 and 286 K. *Zeitschrift f UMLAUTur Kristallographie - Crystalline Materials* **202**, 99–108 (1994).
34. C Groves, E Lewars, Dimers, trimers and oligomers of sulfur oxides: an ab initio and density functional study. *J. Mol. Struct. THEOCHEM* **530**, 265 – 279 (2000).
35. G Frapper, Polysulfite, a hypothetical allotrope of sulfur dioxide? a molecular and periodic quantum investigation of covalent oligomeric and one-dimensional  $\text{SO}_2$ -based compounds ( $x = s, se$ ). *New J. Chem.* **25**, 440–445 (2001).
36. R Wentorf, Chemistry at high pressures, the physics and chemistry of high pressure. *Soc. Chem. Ind. London, S.W. 1*, 185 – 190 (1963).
37. Neuhaus, A., Synthese, Strukturverhalten und Valenzzust nde der anorganischen Materie im Bereich hoher und h ochster Drucke. *Chimia* **18**, 93–103 (1964).
38. CT Prewitt, RT Down, High-pressure crystal chemistry. *Rev. Miner.* **37**, 283–317 (1998).
39. TA Manz, NG Limas, Introducing ddec6 atomic population analysis: part 1. charge partitioning theory and methodology. *RSC Adv.* **6**, 47771–47801 (2016).
40. C Glass, A Oganov, N Hansen, Uspex - evolutionary crystal structure prediction. *Comp. Phys. Comm.* **175**, 713–720 (2006).
41. G Kresse, GJ Hafner, *Ab initio* molecular dynamics for liquid metals. *Phys. Rev. B* **47**, 558–561 (1993).
42. G Kresse, J Furthm ller, Efficiency of ab-initio total energy calculations for metals and semiconductors using a plane-wave basis set. *Comput. Mater. Sci.* **6**, 15 – 50 (1996).
43. G Kresse, J Furthm ller, Efficient iterative schemes for ab initio total-energy calculations using a plane-wave basis set. *Phys. Rev. B* **54**, 11169–11186 (1996).
44. JP Perdew, K Burke, M Ernzerhof, Generalized gradient approximation made simple. *Phys. Rev. Lett.* **77**, 3865–3868 (1996).